

Gradient-Based Predictive Pulse Pattern Control with Optimal Active Neutral Point Potential Balancing for Five-Level Medium-Voltage Drives

Ilari Hilden

Faculty of Inf. Technol. and Commun. Sciences
Tampere University
Tampere, Finland
ilari.hilden@tuni.fi

Petros Karamanakos

Faculty of Inf. Technol. and Commun. Sciences
Tampere University
Tampere, Finland
p.karamanakos@ieee.org

Tobias Geyer

Motion System Drives
ABB Switzerland Ltd
Turgi, Switzerland
t.geyer@ieee.org

Abstract—This paper presents a control algorithm for five-level neutral-point-clamped (NPC) H-bridge medium-voltage (MV) drives. Specifically, a model predictive control (MPC) method is developed to directly manipulate optimized pulse patterns (OPPs) in real time. This enables accurate tracking of the optimal reference trajectory while achieving excellent transient performance. Moreover, owing to the multiple-input multiple-output nature of the proposed controller, the neutral point (NP) potential balancing problem is addressed within the same control loop. To achieve this, the proposed method includes an optimal active NP potential balancing mechanism that ensures minimal NP potential ripple and equal utilization of the switching devices. The effectiveness of the proposed control method is demonstrated on the target MV drive system, and its superior performance is demonstrated through comparisons to existing approaches.

Index Terms—Model predictive control (MPC), optimized pulse patterns (OPPs), medium-voltage (MV) drives, neutral point potential

I. INTRODUCTION

Multilevel converters, such as the five-level neutral-point-clamped (NPC) H-bridge converter [1], are widely used in high-power medium-voltage (MV) applications due to their advantages, including lower harmonic distortion and reduced stress on semiconductor devices [2]. The most common modulation method for these converters is carrier-based pulse width modulation (CB-PWM) [3]. However, since such converters typically operate at switching frequencies of only a few hundred hertz to remain within the thermal cooling capabilities of the converter, the performance of CB-PWM deteriorates, resulting in increased harmonic distortion in the load current. Increasing the switching frequency to improve the current quality is undesirable, as it would lead to significantly higher switching losses and drastically limit the power capability of the converter [4], [5]. To address this issue, optimized pulse patterns (OPPs) can be employed, as they minimize the harmonic distortions at low switching-to-fundamental frequency ratios, i.e., pulse numbers [6].

Achieving fast closed-loop control with OPPs, however, is challenging. Due to the absence of a fixed modulation cycle, OPPs are difficult to utilize in closed-loop systems

with traditional linear controllers. Consequently, OPPs have typically been used with low-bandwidth controllers. Recently, the gradient-based predictive pulse pattern control (GP³C) algorithm has emerged as a versatile and powerful solution for employing OPPs in fast closed-loop control [7]. By leveraging model predictive control (MPC), GP³C optimally manipulates OPPs in real time, ensuring both very low harmonic distortion and fast dynamic performance.

When the five-level NPC H-bridge topology is considered, the controller must meet additional objectives. Most notably, the internal voltages of the dc-link capacitors must be kept balanced to ensure that the neutral point (NP) potential in each phase remains close to zero. To achieve this, control strategies for five-level converters typically exploit their inherent switching state redundancies in real time to drive the NP potential towards zero [8]. However, these methods are prone to persistent NP potential offsets and uneven utilization of the switching devices, resulting in unequal stress distribution and, over time, degradation of device lifetime. Other approaches employ modulation-based techniques to balance the capacitor voltages [5], [9]. These PWM strategies aim at equally utilizing the dc-link capacitors over a certain time period. However, during transients or load imbalances, these methods fail to control the NP potential voltage effectively.

To address these challenges, this paper proposes an *optimal* NP potential balancing strategy. Specifically, the optimal redundant switching states associated with the used OPPs are computed offline and implemented in real time to achieve zero average NP potential voltage with minimal ripple, along with balanced utilization of the switching devices. By exploiting the design versatility and multiple-input multiple-output (MIMO) nature of GP³C, this approach is seamlessly integrated into the GP³C framework, thereby enabling overall superior drive system performance.

II. MODEL OF THE FIVE-LEVEL NPC H-BRIDGE MV DRIVE

The model of the system of interest is done in the orthogonal ($\alpha\beta$) plane. To this end, a variable in the three-phase *abc*-plane

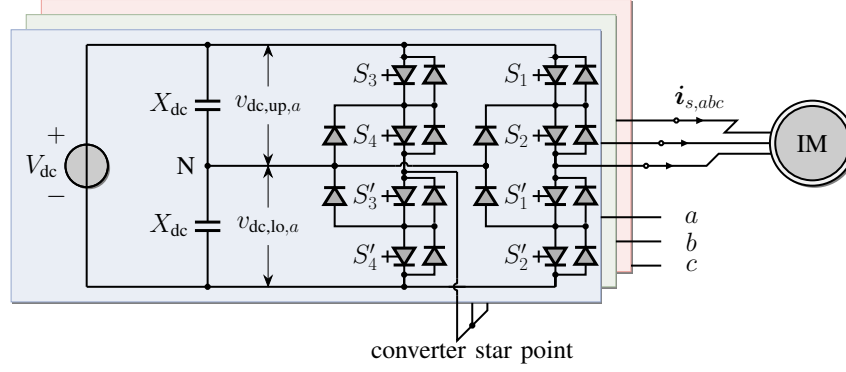


Fig. 1. MV drive with a five-level NPC H-bridge inverter and an induction machine.

TABLE I
SWITCHING STATES OF THE FIVE-LEVEL NPC H-BRIDGE CONVERTER
AND CORRESPONDING OUTPUT VOLTAGE AND SWITCH POSITIONS

S_1	S_2	S_3	S_4	$v_{s,x}$	u_x
1	1	0	0	$v_{dc,up,x} + v_{dc,lo,x}$	2
1	1	0	1	$v_{dc,up,x}$	1
0	1	0	0	$v_{dc,lo,x}$	1
1	1	1	1	0	0
0	1	0	1	0	0
0	0	0	0	0	0
0	0	0	1	$-v_{dc,lo,x}$	-1
0	1	1	1	$-v_{dc,up,x}$	-1
0	0	1	1	$-(v_{dc,up,x} + v_{dc,lo,x})$	-2

ξ_{abc} can be transformed to the $\alpha\beta$ -plane with $\xi_{\alpha\beta} = \mathbf{K}\xi_{abc}$ through the transformation matrix¹

$$\mathbf{K} = \frac{2}{3} \begin{bmatrix} 1 & -\frac{1}{2} & -\frac{1}{2} \\ 0 & \frac{\sqrt{3}}{2} & -\frac{\sqrt{3}}{2} \end{bmatrix}. \quad (1)$$

Additionally, all the quantities in this paper are assumed to be in the per unit (p.u.) system.

A. Converter Modeling

Consider a drive system consisting of a five-level NPC H-bridge converter and an induction machine (IM), see Fig. 1. Each phase of the converter consists of a dc link, with constant voltage V_{dc} and two identical capacitors of reactance X_{dc} , and two three-level NPC legs. The output of the left leg is connected to the star point of the converter, while the output of the right leg is connected to the machine, forming a three-phase connection. In each phase $x \in \{a, b, c\}$, either of the two NPC legs can be connected to the positive rail, the neutral point, or the negative rail, enabling the converter to generate five discrete output voltage levels. These levels correspond to specific single-phase switch positions, modeled with the integer variable $u_x \in \{0, \pm 1, \pm 2\}$, where $u_x = 2$ ($u_x = -2$) indicates that the total positive (negative) dc-link voltage is applied to the output, $u_x = 1$ ($u_x = -1$) indicates that a positive (negative) half of the dc link is applied, and $u_x = 0$ corresponds to both legs being connected to the same potential.

¹In this paper, the $\alpha\beta$ subscript is omitted for the variables in the $\alpha\beta$ -plane. The subscript abc is used for variables in the three-phase abc -plane.

The different switch positions can be realized by selecting the *single-phase* switching state of the converter $\mathbf{s}_x = [S_1 \ S_2 \ S_3 \ S_4]^T$, $S_i \in \{0, 1\}$, $i \in \{1, 2, 3, 4\}$, according to Table I, with S_i being the switching state of the i^{th} switch.² Given the upper and lower dc-link capacitor voltages in phase x , $v_{dc,up,x}$ and $v_{dc,lo,x}$, respectively, with $V_{dc} = v_{dc,up,x} + v_{dc,lo,x}$, the single-phase output—stator—voltage $v_{s,x}$ is then given by

$$v_{s,x} = (v_{dc,up,x}[1 \ 0 \ -1 \ 0] + v_{dc,lo,x}[0 \ 1 \ 0 \ -1])\mathbf{s}_x. \quad (2)$$

It is worth noting that although there are five output voltage levels (i.e., switch positions), these can be generated using nine unique single-phase switching states. Specifically, the switch position $u_x = \pm 1$ can be implemented using two different switching states, while $u_x = 0$ can be realized with three different switching states, as shown in Table I. An example of a such single-phase redundancy for the switch position $u_x = 1$ is shown in Fig. 2.

While the single-phase redundancies do not (substantially) affect the stator voltage, they have a significant impact on the NP potential, defined in phase x as

$$v_{n,x} = \frac{1}{2}(v_{dc,lo,x} - v_{dc,up,x}). \quad (3)$$

The NP potential evolves as a function of the single-phase switching state \mathbf{s}_x and the stator current $i_{s,x}$ according to

$$\frac{dv_{n,x}}{dt} = \frac{1}{2X_{dc}}\mathbf{o}^T \mathbf{s}_x i_{s,x}, \quad (4)$$

where $\mathbf{o} = [1 \ -1 \ -1 \ 1]^T$.

B. Model of the Induction Machine

The dynamics of the squirrel cage IM can be described using the stator current \mathbf{i}_s and the rotor flux ψ_r , i.e.,

$$\frac{d\mathbf{i}_s}{dt} = -\frac{1}{\tau_s}\mathbf{i}_s + \left(\frac{1}{\tau_r} - \omega_r \begin{bmatrix} 0 & -1 \\ 1 & 0 \end{bmatrix} \right) \frac{X_m}{D}\psi_r + \frac{X_r}{D}\mathbf{v}_s, \quad (5a)$$

$$\frac{d\psi_r}{dt} = \frac{X_m}{\tau_r}\mathbf{i}_s - \frac{1}{\tau_r}\psi_r + \omega_r \begin{bmatrix} 0 & -1 \\ 1 & 0 \end{bmatrix} \psi_r. \quad (5b)$$

In (5), $\tau_s = X_r D / (R_s X_r^2 + R_r X_m^2)$ and $\tau_r = X_r / R_r$ are the (transient) stator and rotor time constants, respectively,

²The complementary switching state is $S'_i = 1 - S_i$, see Fig. 1.

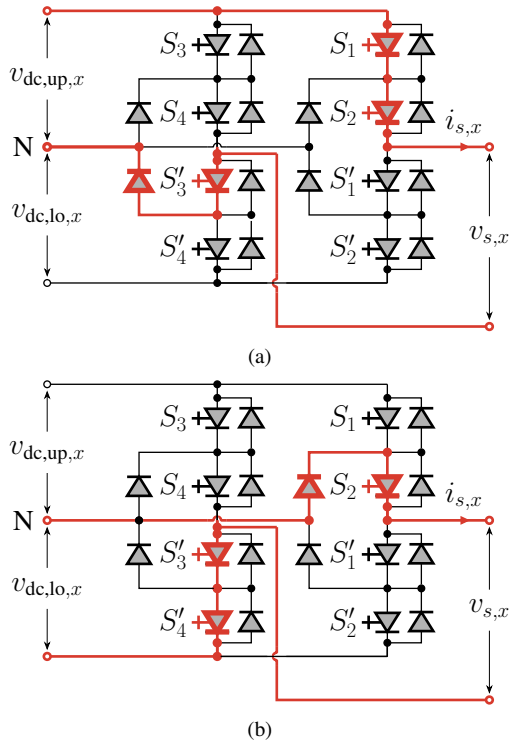


Fig. 2. Example of a single-phase redundancy where the voltage level $u_x = 1$ is implemented using: (a) the upper capacitor $v_{dc,up,x}$; (b) the lower capacitor $v_{dc,lo,x}$. The current path is highlighted in red, assuming a positive stator phase current $i_{s,x}$.

where the stator and rotor self-reactances are $X_s = X_{ls} + X_m$ and $X_r = X_{lr} + X_m$, respectively, with X_{ls} (X_{lr}) being the stator (rotor) leakage reactance, and X_m the mutual reactance. Additionally, R_s is the stator resistance and R_r is the rotor resistance. The constant D is given by $D = X_s X_r - X_m^2$ and \mathbf{I}_2 is the two-dimensional identity matrix. Finally, the rotor angular speed ω_r is considered to be a slowly varying parameter, and therefore, its dynamics are not modeled.

Let the system input be the *three-phase* switching state $\mathbf{s}_{abc} = [s_a^T \ s_b^T \ s_c^T]^T \in \{0, 1\}^{12}$. The state is $\mathbf{x} = [i_{s,\alpha\beta}^T \ \psi_{r,\alpha\beta}^T \ \mathbf{v}_{n,abc}^T]^T \in \mathbb{R}^7$, consisting of the stator current i_s and rotor flux ψ_r in the $\alpha\beta$ -plane, along with the three-phase NP potentials $\mathbf{v}_{n,abc} = [v_{n,a} \ v_{n,b} \ v_{n,c}]^T \in \mathbb{R}^3$. Finally, the output is $\mathbf{y} = [i_s^T \ \mathbf{v}_{n,abc}^T]^T \in \mathbb{R}^5$. With the help of (2), (4) and (5), the continuous-time state-space model of the system is

$$\frac{d\mathbf{x}(t)}{dt} = \mathbf{F}(t)\mathbf{x}(t) + \mathbf{G}\mathbf{s}_{abc}(t), \quad (6a)$$

$$\mathbf{y}(t) = \mathbf{C}\mathbf{x}(t), \quad (6b)$$

with $\mathbf{F}(t) \in \mathbb{R}^{7 \times 7}$, $\mathbf{G} \in \mathbb{R}^{7 \times 12}$, and $\mathbf{C} \in \mathbb{R}^{5 \times 7}$ being the state, input, and output matrices, respectively, provided in Appendix A.

III. OPPS FOR A FIVE-LEVEL H-BRIDGE NPC INVERTER

A. Properties of OPPs

OPPs minimize the load (e.g., stator) current harmonic distortions as quantified by the total demand distortion (TDD).

To achieve this, an offline optimization problem is solved for each modulation index m , with the objective function targeting the load current TDD. To cover the full operating range, this optimization is performed for all possible modulation indices $m \in \{0, 4/\pi\}$ and for several pulse numbers $d \in \mathbb{N}^+$. Additionally, quarter- and half-wave symmetry is imposed on the OPPs, ensuring that the load harmonics appears only at non-triplen odd multiples of the fundamental frequency.

The optimization yields a set of d switching angles $\alpha = [\alpha_1 \ \alpha_2 \ \dots \ \alpha_d] \in [0, \pi/2]^d$ and corresponding $d + 1$ single-phase switch positions $\mathbf{u}_x = [u_0 \ u_1 \ \dots \ u_d] \in \{0, 1, 2\}^{d+1}$ for each (m, d) pair. These are stored in a look-up table (LUT). To generate the full-period single-phase pulse pattern $u_x(\theta)$, the imposed symmetry properties are utilized. The three-phase OPP is then constructed by phase-shifting the single-phase pattern by $2\pi/3$ and $4\pi/3$ to obtain the phase- b and phase- c patterns, respectively.

B. Optimal Redundant Sequence

As shown in Table I, different switching states correspond to the same single-phase switch position, introducing redundancies that affect the NP potential differently. Analysis of Table I and (4) shows that for switch positions $u_x = \pm 1$, the single-phase redundancies have opposite effects on the NP potential. Thus, by selecting appropriate single-phase redundancies, the NP potential can be controlled. Conversely, for $u_x = 0$, the redundancies do not affect the NP potential or the stator voltage, therefore, only the switching state $\mathbf{s}_x = [0 \ 1 \ 0 \ 1]^T$ is considered when realizing this switch position.³

When selecting single-phase redundancies, factors beyond the NP potential balancing must be considered, such as the impact on load current harmonics and switching device utilization. In [10], the concept of pattern interchange was proposed as a strategy to utilize all the switching devices equally. In pattern interchange, the single-phase redundancies are reversed every fundamental period, meaning the three-level pulse patterns of the two NPC legs forming the five-level pattern are interchanged each period, as illustrated in Fig. 3. This ensures equal average switching frequency between the two legs, even with odd pulse numbers, which result in non-integer switching-to-fundamental frequency ratios for the three-level patterns over a single period. Consequently, thermal stress is evenly distributed among the switching devices, increasing the converter power capability [5]. Finally, it is worth mentioning that although this strategy introduces additional harmonic distortions, it has been shown that eventually the load current quality does not significantly degrade [11].

Due to the periodicity of the three-level pulse patterns from pattern interchange, the NP potential does not drift but only oscillates with a period twice the fundamental. However, within a single fundamental period, the NP potential should remain as close to zero as possible for optimal drive performance.

³Additional redundant single-phase switching states can be used to minimize commutations, but this is not considered in this work.

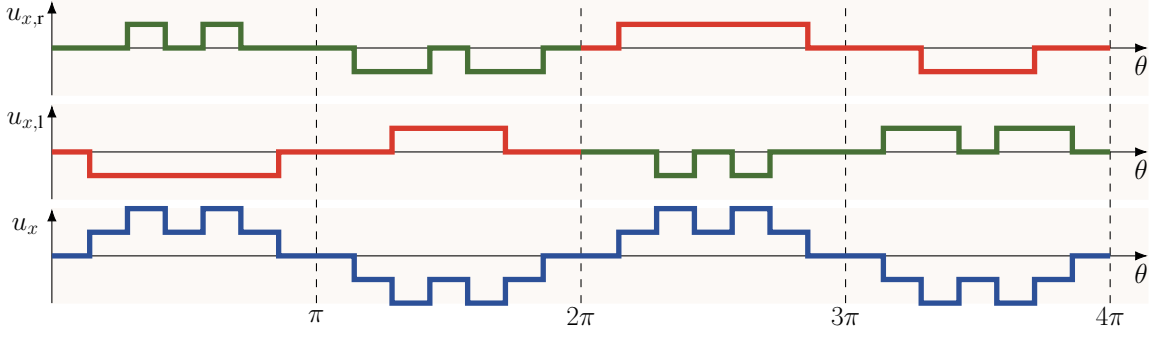


Fig. 3. Example of pattern interchange. The phase- x switch position u_x is generated as the difference between the switch position of the right and left NPC legs, $u_{x,r}$ and $u_{x,l}$, respectively, i.e., $u_x = u_{x,r} - u_{x,l}$. To achieve equal utilization of the switching devices, the two three-level pulse patterns (red and green) are interchanged between the two legs every fundamental period.

Assuming a sinusoidal stator current, integrating (4) yields the NP potential in phase x

$$v_{n,x}(\theta) = \frac{I_s}{2X_{dc}} \int_0^\theta \mathbf{o}^T \mathbf{s}_x(\theta) \sin(\theta + \phi) d\theta, \quad (7)$$

where I_s is the stator current magnitude and ϕ is the displacement angle between the stator voltage and current. The switching function $\mathbf{s}_x(\theta)$ is piecewise constant. It is defined by the d switching angles α of the OPP, the corresponding switching states \mathbf{s}_x , and the initial state $\mathbf{s}_x(0) = [0 \ 1 \ 0 \ 1]^T$, since $u_x = 0$ holds by design of the OPP. As mentioned before—and as can be inferred from Table I and (4)—the OPP switch positions $u_x \in \{-2, 0, 2\}$ do not affect the NP potential, i.e., $\mathbf{o}^T \mathbf{s}_x = 0$. However, when $u_x = \pm 1$, the NP potential changes, with the corresponding phase-level redundancies affecting it in opposite directions. To facilitate the modeling of the NP potential the variable $g \in \{-1, 0, 1\}$ is introduced, where $g = 1$ ($g = -1$) denotes the switching state that increases (decreases) the NP potential, while $g = 0$ denotes a state with no impact on it. With these definitions, the NP potential (7) at the $4d$ switching angles $\alpha_\ell, \ell \in \{1, 2, \dots, 4d\}$, over one fundamental period can be written as

$$v_{n,x}(\alpha_\ell) = \frac{I_s}{2X_{dc}} \sum_{i=1}^{\ell} g_{i-1} \int_{\alpha_{i-1}}^{\alpha_i} \sin(\theta + \phi) d\theta \quad (8)$$

where $\alpha_0 = 0$. Evaluating the integrals, (8) becomes

$$v_{n,x}(\alpha_\ell) = \frac{I_s}{2X_{dc}} \left(\sum_{i=1}^{\ell} g_{i-1} (\cos(\alpha_{i-1} + \phi) - \cos(\alpha_i + \phi)) + K \right) \quad (9)$$

where $K \in \mathbb{R}$ is the integration constant.

To achieve minimal ripple in the NP potential, the *optimal* redundant switching states are determined in an offline optimization procedure that minimizes the (approximate) energy of the NP potential over one fundamental period. The latter is captured by the following objective function

$$J_{v_n} = \sum_{i=1}^{2d} v_{n,x}^2(\alpha_i). \quad (10)$$

It is important to note that only the $2d$ switching angles that correspond to witch positions $u_x = \pm 1$ (i.e., those assigned to $g \pm 1$) are considered in (10) as only these affect the NP potential (see (8)). With some algebraic manipulations—provided in Appendix B—function (10) can be written in the compact vector form

$$J_{v_n} = \mathbf{g}^T \mathbf{P}(\phi) \mathbf{g}, \quad (11)$$

where the vector $\mathbf{g} \in \{1, -1\}^{2d}$ collects the $2d$ single-phase redundancies within a fundamental period and $\mathbf{P} \in \mathbb{R}^{2d \times 2d}$ is an upper diagonal matrix that depends on the switching angles α_ℓ and the displacement angle ϕ .

The dependence on the displacement angle ϕ implies that an optimal redundant sequence needs to be computed for each pair of modulation index m and displacement angle ϕ . This, however, would result in a large amount of data to be stored. To avoid this, the matrix \mathbf{P} is averaged over a range of displacement angles $\phi \in [0, \pi/2]$. With the averaging, the objective function becomes

$$J_{v_n, \text{avg}} = \frac{1}{N} \sum_{j=1}^N \mathbf{g}^T \mathbf{P}(\phi_j) \mathbf{g} = \mathbf{g}^T \mathbf{P}_{\text{avg}} \mathbf{g}, \quad (12)$$

with $\mathbf{P}_{\text{avg}} = (\mathbf{P}(\phi_1) + \mathbf{P}(\phi_2) + \dots + \mathbf{P}(\phi_N))/N$, and $N \in \mathbb{N}^+$ being the number of discrete samples of ϕ .

Based on (12), the optimization problem that yields the optimal redundant switching states \mathbf{g}^* is formulated as

$$\begin{aligned} & \underset{\mathbf{g}}{\text{minimize}} && \mathbf{g}^T \mathbf{P}_{\text{avg}} \mathbf{g} \\ & \text{subject to} && \mathbf{g} \in \{-1, 1\}^{2d}. \end{aligned} \quad (13)$$

Problem (13) is solved for each (m, d) pair, similarly to the OPP optimization problem, and the results are stored in a LUT. In addition, with the knowledge of the optimal redundant switching states \mathbf{g}^* —and thus the switching function $\mathbf{s}(\theta)$ for a given OPP—the optimal NP potential references can be computed with the help of (7) and stored in a LUT. These references are then used by the GP³C algorithm discussed in the following section.

IV. GP³C WITH ACTIVE NP POTENTIAL BALANCING

The GP³C algorithm [7] combines MPC with OPPs to achieve excellent steady-state and dynamic performance for

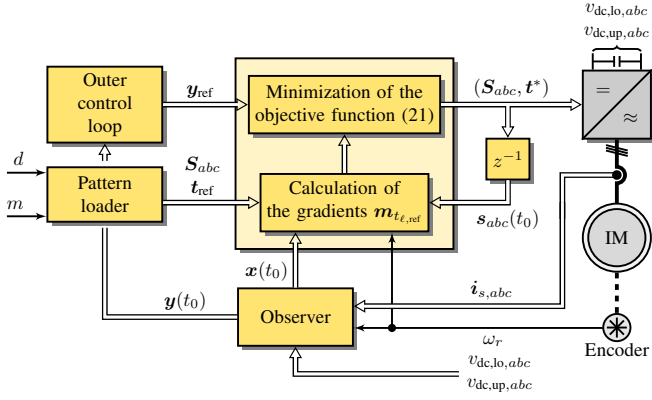


Fig. 4. Block diagram of the proposed GP³C algorithm.

complex power electronic systems. In this section, GP³C is tailored to control the five-level H-bridge NPC MV drive system. Specifically, GP³C is used to control the stator current i_s and the three-phase NP potential $v_{n,abc}$. The latter is directly addressed in the GP³C control problem because, although the optimal redundant sequences described in Section III can guarantee zero average NP potential over two fundamental periods, they cannot provide fast and accurate NP potential balancing during transients or in the presence of external disturbances, such as dc-link voltage ripple.

A. Control Problem

The objective of the GP³C algorithm is to regulate the output \mathbf{y} along its *optimal* reference trajectory \mathbf{y}_{ref} by manipulating the OPP in real time. This ensures minimal harmonic distortion at steady state, fast settling times, and excellent disturbance rejection. To achieve this, the $z \in \mathbb{N}^+$ OPP switching time instants (i.e., switching angles) within the prediction horizon $T_p = N_p T_s$ are dynamically adjusted to eliminate the output tracking error, where N_p is the number of prediction steps and T_s is the sampling interval.

The nominal OPP switching time instants are collected in the vector

$$\mathbf{t}_{ref} = [t_{1,ref} \ t_{2,ref} \ \dots \ t_{z,ref}]^T \in \mathbb{R}^z, \quad (14)$$

while the vector

$$\mathbf{t} = [t_1 \ t_2 \ \dots \ t_z]^T \in \mathbb{R}^z \quad (15)$$

contains the corresponding (to-be-computed) modified instants within T_p . The control objectives described above can be captured with the objective function

$$J = \sum_{i=1}^z \|\mathbf{y}_{ref}(t_{i,ref}) - \mathbf{y}(t_i)\|_{\mathbf{Q}}^2 + \lambda_t \|\Delta \mathbf{t}\|_2^2. \quad (16)$$

In (16), the first term accounts for the weighted (squared) output tracking error over the prediction horizon T_p . The second term models the control effort by penalizing the deviation of the to-be-computed switching time instants from their nominal values, i.e., $\Delta \mathbf{t} = \mathbf{t}_{ref} - \mathbf{t}$. Finally, $\mathbf{Q} \in \mathbb{R}^{5 \times 5}$ and $\lambda_t \in \mathbb{R}$ are tuning parameters. The positive definite matrix $\mathbf{Q} = \text{diag}(\mathbf{I}_2 q_{i_s}, \mathbf{I}_3 q_{v_n})$ is used to set the tracking priority

among the different output variables, where q_{i_s} and q_{v_n} weigh the stator current and three-phase NP potential reference tracking errors, respectively. \mathbf{I}_p denotes a p -dimensional identity matrix. The parameter $\lambda_t > 0$ determines the operating point on the trade-off between output tracking accuracy and controller effort.

B. Control Strategy

To minimize the objective function (16), the output at the modified switching time instants t_ℓ , $\ell \in \{0, 1, 2, \dots, z-1\}$ must be computed. To this end, gradient-based predictions are utilized within each subinterval

$$\Delta t_{\ell,ref} = t_{\ell+1,ref} - t_{\ell,ref} \ll T_1, \quad (17)$$

where T_1 is the fundamental period and the $t_{0,ref} \equiv t_0$ is the current time, i.e., the beginning of the prediction horizon. Given that—due to the offline OPP optimization—the three-phase switching states at the nominal switching time instants are known, i.e.,

$$\mathbf{S}_{abc} = [\mathbf{s}_{abc}^T(t_0) \ \mathbf{s}_{abc}^T(t_{1,ref}) \ \dots \ \mathbf{s}_{abc}^T(t_{z,ref})]^T \in \mathbb{R}^{12(z+1)}, \quad (18)$$

the output at these instants can be predicted iteratively. This is achieved by discretizing model (6) over the subintervals $\Delta t_{\ell,ref}$ resulting in the discrete-time state-space model

$$\mathbf{x}(t_{\ell+1,ref}) = \mathbf{A}\mathbf{x}(t_{\ell,ref}) + \mathbf{B}\mathbf{s}_{abc}(t_{\ell,ref}), \quad (19a)$$

$$\mathbf{y}(t) = \mathbf{C}\mathbf{x}(t_{\ell+1,ref}). \quad (19b)$$

Note that due to the constant switching state \mathbf{s}_{abc} within each subinterval, the system matrix \mathbf{A} is time-invariant. By predicting the output at $t_{\ell,ref}$, the computation of the gradients

$$\mathbf{m}(t_{\ell,ref}) \approx \frac{\mathbf{y}(t_{\ell+1,ref}) - \mathbf{y}(t_{\ell,ref})}{\Delta t_{\ell,ref}}, \quad (20)$$

which describe the output evolution within each subinterval $\Delta t_{\ell,ref}$, is facilitated.

With the help of the gradients $\mathbf{m}(t_{\ell,ref})$, the objective function (16) can be formulated in the compact form

$$J = \|\mathbf{r} - \mathbf{M}\mathbf{t}\|_{\mathbf{Q}}^2 + \lambda_t \|\Delta \mathbf{t}\|_2^2, \quad (21)$$

where the vector \mathbf{r} depends on the references and measurements of the output, while the nonzero entries of matrix \mathbf{M} depend on the gradients with which the controlled variables evolve over the prediction horizon T_p . The output gradient matrix \mathbf{M} , and the reference vector \mathbf{r} have variable dimensions and are computed in real time at each controller iteration.

With (21), the GP³C optimal control problem is written as

$$\begin{aligned} & \underset{\mathbf{t}}{\text{minimize}} \quad \|\mathbf{r} - \mathbf{M}\mathbf{t}\|_{\mathbf{Q}}^2 + \lambda_t \|\Delta \mathbf{t}\|_2^2 \\ & \text{subject to} \quad kT_s < t_1 < \dots < t_z < kT_s + T_p. \end{aligned} \quad (22)$$

Solving (22) yields the *optimal* modified switching time instants \mathbf{t}^* within T_p . Nevertheless, as per the receding horizon policy, only the switching states \mathbf{s}_{abc} that fall within the first T_s of T_p are applied. The block diagram of the controller is presented in Fig. 4. For a more detailed description, along with the derivation of (21) as well as \mathbf{M} and \mathbf{r} , see [7].

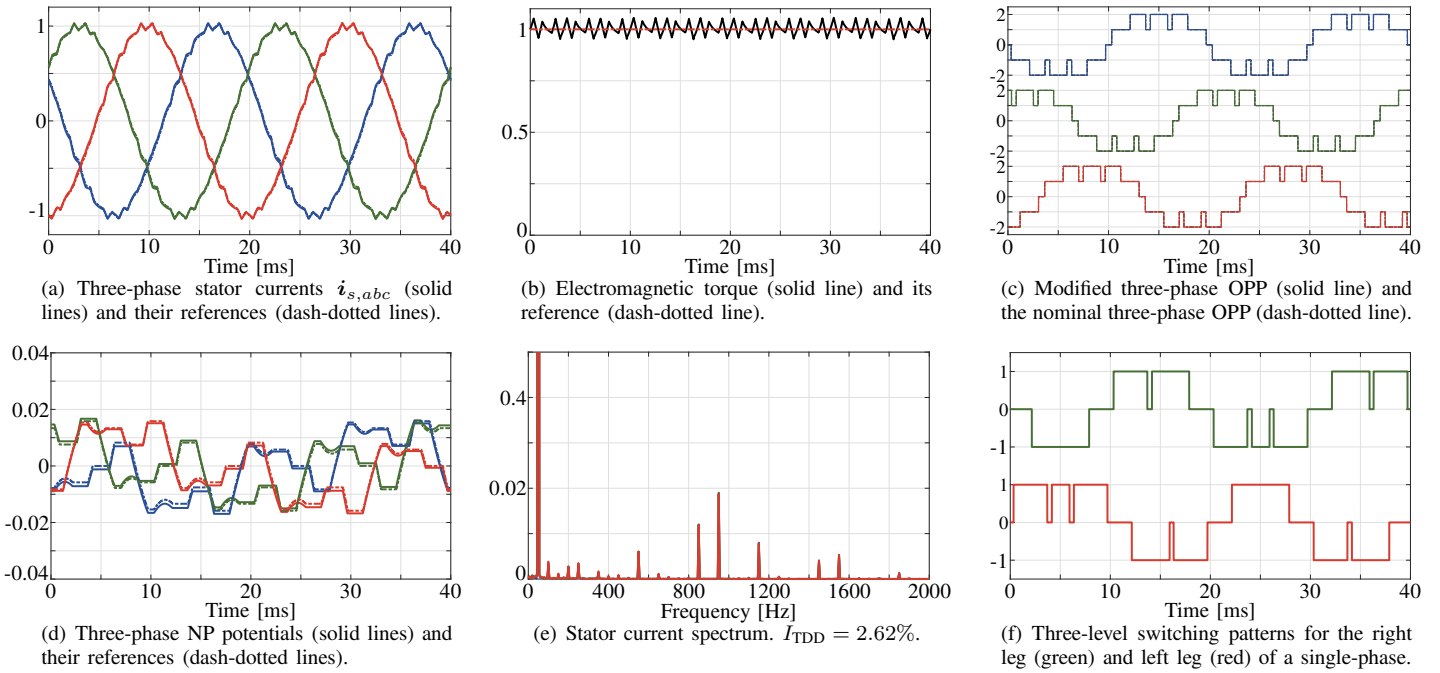


Fig. 5. Steady-state performance of GP³C with the proposed optimal active NP potential balancing approach.

TABLE II
RATED VALUES OF THE INDUCTION MACHINE

Parameter	Symbol	SI value
Voltage	V_R	5389 V
Current	I_R	1485 A
Apparent power	S_R	12 MVA
Stator frequency	ω_{sR}	$2\pi 50$ rad/s
Rotational speed	ω_{mR}	1490 rpm

TABLE III
SYSTEM PARAMETER VALUES IN THE P.U. SYSTEM

Parameter	Symbol	p.u.
Stator resistance	R_s	0.0054
Rotor resistance	R_r	0.0066
Stator leakage reactance	X_{ls}	0.1299
Rotor leakage reactance	X_{lr}	0.1105
Mutual reactance	X_m	4.3496
Dc-link voltage	V_{dc}	0.9620
Dc-link capacitor reactance	X_{dc}	4.4464

V. PERFORMANCE EVALUATION

The proposed GP³C scheme is evaluated through simulations on a 12 MVA five-level NPC H-bridge drive system, see Fig. 1. The rated values of the IM are shown in Table II, while the system parameters are provided in Table III. From these tables, it can be deduced that the total leakage reactance is $X_\sigma = 0.24$ p.u. The controller parameters are as follows: the sampling interval is $T_s = 50 \mu\text{s}$ and the

prediction horizon has $N_p = 15$ steps. The weighting factors are $Q = \text{diag}(1, 1, 20, 20, 20)$ and $\lambda_t = 5 \cdot 10^5$. A five-level OPP with a pulse number $d = 4$ is used. Finally, all results are shown in the p.u. system.

The steady-state performance of the proposed control strategy is shown in Fig. 5 when operating at nominal torque and rated speed. As can be observed, the stator current tracking performance of GP³C is excellent, with minimal deviations from the optimal reference trajectory, yielding a stator current TDD of only $I_{TDD} = 2.62\%$. Moreover, thanks to the symmetry properties of the OPP, the harmonic power is concentrated at the non-triplen odd multiples of the fundamental frequency, as seen in Fig. 5(e). Regarding the NP potential balancing, Fig. 5(d) shows that the three-phase NP potentials accurately track their references, thus staying very close to zero potential. Additionally, due to pattern interchange, the period of the NP potential is twice the fundamental period, i.e., 40 ms. This phenomenon leads to additional 2nd and 4th harmonics in the stator current (see Fig. 5(e)), both of which are negligible in magnitude, being less than 0.5% of the fundamental. However, as shown in Fig. 5(f), thanks to pattern interchange, all devices operate at a switching frequency of $f_{sw} = 100$ Hz, thus distributing the thermal stress evenly between the two NPC legs in each phase.

For comparison purposes, Fig. 6 shows GP³C with the active NP potential balancing method from [8]. With such balancing methods, which select the switching state in real time, the switching devices may experience a switching frequency discrepancy of up to 100 Hz between the two NPC legs, as shown in Fig. 6(c), where the switching frequencies for the left and right NPC legs are 150 Hz and 50 Hz, respectively. Moreover, the peak-to-peak NP potential ripple (see Fig. 6(a))

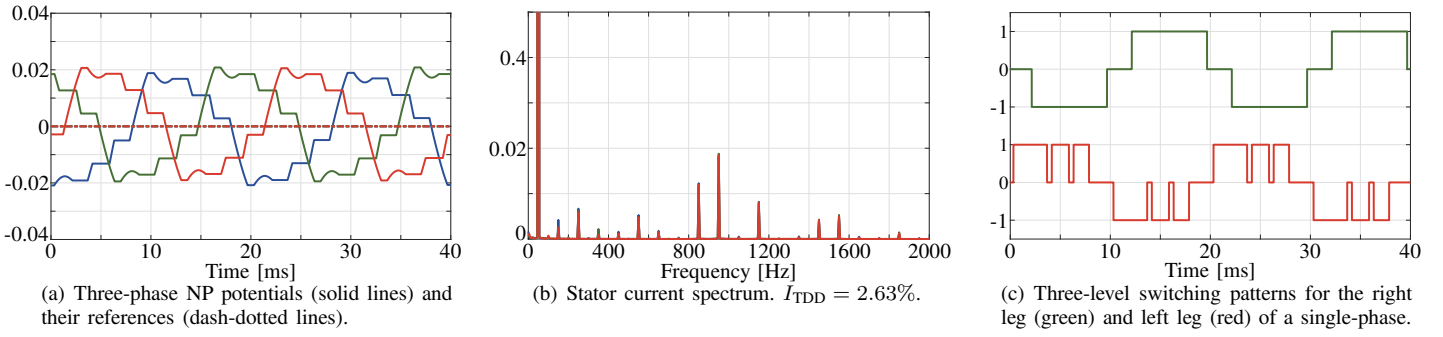


Fig. 6. Steady-state performance of GP³C with the active NP potential balancing method from [8].

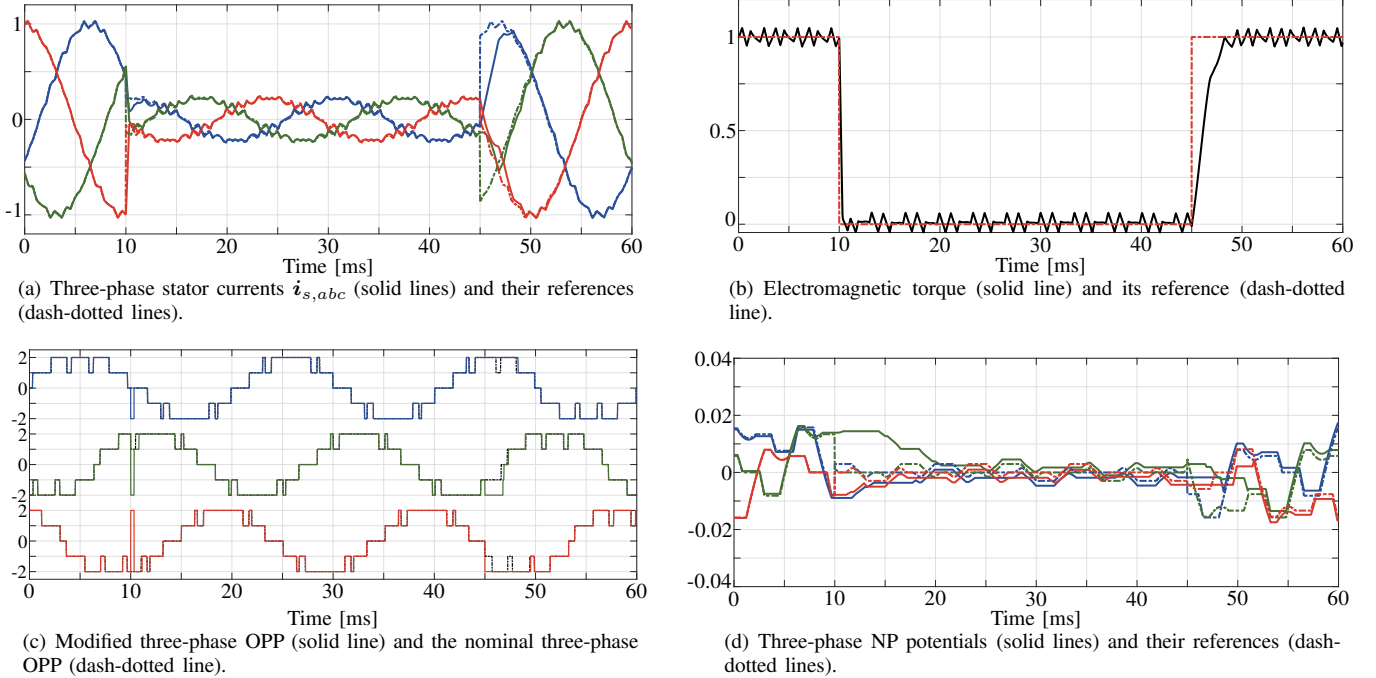


Fig. 7. Transient performance of GP³C with the proposed optimal active NP potential balancing approach.

is larger than what is achieved with the proposed optimal balancing method, while the stator current TDD is similar between the methods due to the same OPP being used.

The transient performance of the proposed control scheme is illustrated in Fig. 7. During operation at nominal speed, the electromagnetic torque reference is stepped down from $T_{e,ref} = 1$ to 0 p.u. at $t = 10$ ms and restored at $t = 45$ ms. As can be seen, the controller quickly regulates the output variables along their respective references, resulting in fast torque responses. This is achieved by employing three-phase pulse insertion [12] and significantly modifying the nominal OPP. Additionally, as shown in Fig. 7(d), the NP potentials are kept balanced despite substantial changes in the stator currents. Notably, even when the stator current is drastically reduced, implying limited ability to eliminate large NP potential deviations, GP³C very quickly drives the NP potentials towards their respective references.

VI. CONCLUSIONS

This paper adapted the GP³C algorithm presented in [7] to five-level NPC H-bridge MV drives. To this end, the controller is augmented with an active NP potential balancing mechanism that selects the optimal switching redundancies via an offline optimization procedure. As demonstrated by the results, thanks to the combination of MPC, offline-computed optimal modulation, and the optimal redundant switching sequences, the proposed approach achieves excellent performance in both steady-state and transient conditions, while balancing the NP potential with minimal ripple. Additionally, by employing pattern interchange, uniform utilization of the switching devices is achieved, thus ensuring uniform thermal stress distribution.

ACKNOWLEDGMENT

This work was supported by the Research Council of Finland.

APPENDIX A
CONTINUOUS-TIME STATE-SPACE MATRICES

The matrices in (6) are

$$\mathbf{F}(t) = \begin{bmatrix} \mathbf{F}_{\text{IM}} & \begin{bmatrix} \frac{X_r}{D} \mathbf{K} \begin{bmatrix} \mathbf{o}_2^T \mathbf{s}_a(t) \\ \mathbf{o}_2^T \mathbf{s}_b(t) \\ \mathbf{o}_2^T \mathbf{s}_c(t) \end{bmatrix} \\ \mathbf{0}_{2 \times 3} \end{bmatrix} \\ \begin{bmatrix} \frac{1}{2X_{\text{dc}}} \begin{bmatrix} \mathbf{o}^T \mathbf{s}_a(t) \\ \mathbf{o}^T \mathbf{s}_b(t) \\ \mathbf{o}^T \mathbf{s}_c(t) \end{bmatrix} \mathbf{K}^{-1} & \mathbf{0}_{3 \times 2} \end{bmatrix} & \mathbf{0}_{3 \times 3} \end{bmatrix},$$

$$\mathbf{G} = \frac{V_{\text{dc}} X_r}{2D} \begin{bmatrix} \mathbf{K}(\mathbf{I}_3 \otimes \mathbf{o}_3^T) \\ \mathbf{0}_{5 \times 12} \end{bmatrix}, \quad \mathbf{C} = \begin{bmatrix} \mathbf{I}_2 & \mathbf{0}_{2 \times 5} \\ \mathbf{0}_{3 \times 2} & \begin{bmatrix} \mathbf{0}_{3 \times 2} & \mathbf{I}_3 \end{bmatrix} \end{bmatrix},$$

where \mathbf{o}_2 and \mathbf{o}_3 are the vectors

$$\mathbf{o}_2 = [-1 \quad 1 \quad 1 \quad 1]^T$$

$$\mathbf{o}_3 = [1 \quad 1 \quad -1 \quad -1]^T,$$

and \mathbf{F}_{IM} is the system matrix of the IM, i.e.,

$$\mathbf{F}_{\text{IM}} = \begin{bmatrix} -\frac{1}{\tau_s} & 0 & \frac{X_m}{\tau_r D} & \omega_r \frac{X_m}{D} \\ 0 & -\frac{1}{\tau_s} & -\omega_r \frac{X_m}{D} & \frac{X_m}{\tau_r D} \\ \frac{X_m}{\tau_r} & 0 & -\frac{1}{\tau_r} & -\omega_r \\ 0 & \frac{X_m}{\tau_r} & \omega_r & -\frac{1}{\tau_r} \end{bmatrix}.$$

APPENDIX B
DESCRIPTION OF OBJECTIVE FUNCTION (11)

The requirement of 4π -periodicity and half-wave symmetry, i.e., $v_{n,x}(0) = -v_{n,x}(2\pi)$, defines the integration constant K in (9) as

$$K = -\frac{v_{n,x}(2\pi)}{2}.$$

Therefore, when considering one fundamental period of the OPP and the switch positions that affect the NP potential, i.e., $u_x = \pm 1$, the NP potential at switching angle α_i , with $i \in \{1, 2, \dots, 2d\}$, is given by

$$v_{n,x}(\alpha_i) = \frac{I_s}{2X_{\text{dc}}} \left(\sum_{j=1}^i g_{j-1} c_j - \underbrace{\frac{1}{2} \sum_{j=1}^{2d} g_{j-1} c_j}_K \right)$$

with $c_j = \cos(\alpha_{j-1} + \phi) - \cos(\alpha_j + \phi)$. When deriving the desired objective function, the constant $\frac{I_s}{2X_{\text{dc}}}$ can be omitted as it does not affect the solution. Thus, (10) becomes

$$J_{v_n} = \sum_{i=1}^{2d} \left(\sum_{j=1}^i g_{j-1} c_j - \frac{1}{2} \sum_{j=1}^{2d} g_{j-1} c_j \right)^2.$$

By expanding and rearranging the terms in the above expression, the objective function can be written in the vector form see (11)

$$J = \mathbf{g}^T \mathbf{P}(\phi) \mathbf{g},$$

with

$$\mathbf{P} = \begin{bmatrix} dc_1^2 & (2d-2)c_1c_2 & (2d-4)c_1c_3 & \cdots & (-2d+2)c_{2d-1}c_{2d} \\ 0 & dc_2^2 & (2d-2)c_2c_3 & \cdots & (-2d+4)c_{2d-2}c_{2d-1} \\ \vdots & \vdots & \vdots & \ddots & \vdots \\ 0 & 0 & 0 & 0 & dc_{2d}^2 \end{bmatrix}.$$

REFERENCES

- [1] C. Wu, W. Lau, and H. Chung, "A five-level neutral-point-clamped H-bridge PWM inverter with superior harmonics suppression: A theoretical analysis," in *Proc. IEEE Int. Symp. Circuits Syst.*, Orlando, FL, USA, May/Jun. 1999, pp. V-198–V-201.
- [2] K. Gupta, R. Ranjan, P. Bhatnagar, L. Sahu, and S. Jain, "Multilevel inverter topologies with reduced device count: A review," *IEEE Trans. Power Electron.*, vol. 31, no. 1, Jan. 2016.
- [3] D. G. Holmes and T. A. Lipo, *Pulse width modulation for power converters: Principles and practice*. Piscataway, NJ, USA: IEEE Press, 2003.
- [4] J. Shen, S. Schröder, H. Stagege, and R. W. D. Doncker, "Impact of modulation schemes on the power capability of high-power converters with low pulse ratios," *IEEE Trans. Power Electron.*, vol. 29, no. 11, pp. 5696–5705, Nov. 2014.
- [5] J. Shen, S. Schröder, B. Qu, Y. Zhang, K. Chen, F. Zhang, and R. Zhang, "Modulation schemes for a 30-MVA IGCT converter using NPC H-bridges," *IEEE Trans. Ind. Appl.*, vol. 51, no. 5, pp. 4028–4040, Sep./Oct. 2015.
- [6] G. S. Buja, "Optimum output waveforms in PWM inverters," *IEEE Trans. Ind. Appl.*, vol. IA-16, no. 6, pp. 830–836, Nov./Dec. 1980.
- [7] M. A. W. Begh, P. Karamanakos, and T. Geyer, "Gradient-based predictive pulse pattern control of medium-voltage drives—Part I: Control, concept, and analysis," *IEEE Trans. Power Electron.*, vol. 37, no. 12, pp. 14 222–14 236, Dec. 2022.
- [8] T. Geyer and G. Papafotiou, "Model predictive direct torque control of a variable speed drive with a five-level inverter," in *Proc. IEEE Ind. Electron. Conf.*, Porto, Portugal, Feb. 2009, pp. 1203–1208.
- [9] P. Chamarithi, U. Muduli, M. Moursi, A. Al-Durra, A. Al-Sumaiti, and A. Hosani, "Improved PWM approach for cascaded five-level NPC H-bridge configurations in multilevel inverter," *IEEE Trans. Ind. Appl.*, vol. 60, no. 5, pp. 7048–7060, Sep./Oct. 2024.
- [10] J. Holtz and N. Oikonomou, "Optimal control of a dual three-level inverter system for medium-voltage drives," *IEEE Trans. Ind. Appl.*, vol. 46, no. 3, pp. 1034–1041, May/Jun. 2010.
- [11] J. Shen, S. Schröder, J. Gao, and B. Qu, "Impact of dc-link voltage ripples on the machine-side performance in NPC H-bridge topology," *IEEE Trans. Ind. Appl.*, vol. 52, no. 4, pp. 3212–3223, Jul./Aug. 2016.
- [12] I. Hilden, P. Karamanakos, and T. Geyer, "Gradient-based predictive pulse pattern control for medium-voltage drives with very fast transients," in *Proc. IEEE Energy Convers. Congr. Expo.*, Phoenix, AZ, USA, Oct. 2024, pp. 4283–4285.